ture of many neurological disorders including stroke, spinal cord injury, and ALS (*2*). Excitotoxicity is one of the best links between the rare familial form of ALS (caused by mutations in the gene encoding superoxide dismutase) and the more common sporadic form of this disease (*3*). This realization came from studies in the early 1990s that showed increased glutamate in the fluid surrounding the brain and spinal cord of patients with sporadic ALS (*4*, *5*). Similarly, in a rat model of familial ALS, animals develop focal loss of the EAAT2 glutamate transporter in regions of the spinal cord that house motor neurons (*6*). Indeed, the only approved medication for treating ALS, the drug riluzole, is thought to act by limiting synaptic glutamate release. The effectiveness of this drug, however, has been disappointing, extending survival of ALS patients by a mere 3 months (*7*).

The remarkable discovery by Rothstein and co-workers offers renewed hope for a more effective therapy for ALS and other neurological diseases. A ceftriaxone-induced increase in expression of glutamate transporters by astroctyes enhanced the clearance of glutamate in spinal cord explants and, more important, slowed loss of muscle strength and modestly extended survival of ALS mice. Any benefit from increased glutamate clearance also extends to other types of neuronal damage with an excitotoxic component—for example, the damage that accompanies decreased blood flow typical of stroke (frequently referred to as ischemia). A ceftriaxone-mediated increase in glutamate clearance also decreased neuronal death induced by oxygen deprivation, at least in cell culture.

The encouraging preclinical data from the ALS mouse and other models of neurological disease have prompted a clinical trial combining all three phases. This is expected to begin this spring with a safety and efficacy study of ceftriaxone in the treatment of ALS. The data generated by the consortium represent a phenomenally quick turnaround from initial drug screening (started in early 2002) to actual use in patients. This reflects the major advantage of screening FDA-approved drugs whose safety profiles are already known. Even more encouraging for the Rothstein *et al.* findings are the excellent safety profiles of the β-lactam antibiotics in humans. Drug toxicity is costly and time-consuming to exclude and, in the end, is often the Achilles' heel that sinks the development of promising new therapeutics. In addition, spotting unwanted side effects is challenging even after undertaking multiple preclinical and clinical trials. This lesson was learned most recently with the realization of the increased risk of stroke and heart attack in people taking commonly prescribed anti-inflammatory drugs (*8*). Against this backdrop are the β-lactam antibiotics, first identified with the discovery of penicillin in 1928 and now among the most widely used modern pharmaceuticals. Although data about the safety of long-term ceftriaxone use still need to be collected, the best predictor of safety is a long history of safe use in humans. Our vast experience with short-term β-lactam antibiotic treatment predicts that very few problems should arise over the long term.

The discovery of new modes of action for the β-lactam antibiotic family offers two additional lessons for biomedical researchers. The first is unproven but predictable: A systematic screen of easily accessible chemical compounds already approved by the FDA may reveal common therapeutics with new potential applications. The second is more surprising: Some of these compounds may act by transcriptional induction of key proteins. Searching for transcriptional up-regulation is not an approach generally thought attractive in drug screening. With that in mind, last century's miracle drug, the β-lactams, may well rise to one of the big challenges of this century: slowing the progression of neurological diseases whose treatment has so far evaded the world's best efforts.

References
1. J. D. Rothstein *et al.*, *Nature* **433**, 73 (2005).
2. M. P. Mattson, *Neuromol. Med.* **3**, 65 (2003).
3. P. R. Heath, P. J. Shaw, *Muscle Nerve* **26**, 438 (2002).
4. J. D. Rothstein *et al.*, *Ann. Neurol.* **28**, 18 (1990).
5. J. D. Rothstein *et al.*, *Ann. Neurol.* **30**, 224 (1991).
6. D. S. Howland *et al.*, *Proc. Natl. Acad. Sci. U.S.A.* **99**, 1604 (2002).
7. L. I. Bruijn *et al.*, *Annu. Rev. Neurosci.* **27**, 723 (2004).
8. E. J. Topol, *N. Engl. J. Med.* **351**, 1707 (2004).

GEOSCIENCE

The Boon and Bane of Radiocarbon Dating

Tom P. Guilderson, Paula J. Reimer, Tom A. Brown

Radiocarbon (^{14}C) dating (*1*, *2*) is widely used to determine the ages of samples that are less than about 50,000 years old. Natural radiocarbon is mainly formed in Earth's stratosphere through the interaction of neutrons produced by cosmic rays with 14-nitrogen. However, the rate of radiocarbon production is not constant (*3*), nor is its partitioning among the atmosphere, terrestrial biosphere, and oceans. After local corrections [see, for example, (*4*–*6*)], radiocarbon ages must therefore be calibrated to obtain ages on an absolute time scale (*7*). For decades, the radiocarbon community has adopted international calibration standards, most recently IntCal98 (*8*). Here, we discuss the inherent limitations faced when using radiocarbon dates to derive calendar ages.

From modern day to 11,800 years ago, IntCal98 is based on sets of tree-ring chronologies that each cover several thousand years and together provide an annually resolved, nearly absolute time frame. These data set a quality standard against which other proposed calibration datasets can be judged. Prior to 11,800 years ago, IntCal98 is based on marine data and contains additional assumptions and uncertainties associated with the translation of marine data into atmospheric radiocarbon values.

Here we examine how precisely calendar ages can be determined from individual radiocarbon dates. We focus on the tree-ring section of the IntCal98 calibration curve. Between 0 and 8000 years before the present (B.P.), the error in this curve is often less than 20 years, and—except for a few brief intervals—it is less than 30 years over the past 11,800 years. But as we will show, the range of statistically possible calendar ages, or calibrated age ranges, corresponding to any particular radiocarbon date can be larger or smaller, depending on where it falls on the curve.

We have linearly interpolated the Int-Cal98 curve at intervals of 20 calendar years and determined the radiocarbon dates that correspond to the calendar ages. We then calibrated these resampled radiocarbon ages using CALIB v4.4 (*4*) assuming an uncertainty of ±40 radiocarbon years, which is currently typical of routine dating (calibration 1). We performed a second calibration with a constant uncertainty of ±15 radiocarbon years, which is typical of the IntCal98 tree-ring data (calibration 2).

The calibrated age range waxes and wanes (see the first figure) as a result of variations in the atmospheric ^{14}C/^{12}C ratio. On average, the 1σ calibrated age range is 180 years (minimum 30 years, maximum 529 years) for calibration 1 and 140 years

The authors are at the LLNL Center for Accelerator Mass Spectrometry, University of California, Livermore, CA 94550, USA. T. P. Guilderson is also at the Institute of Marine Science and Department of Ocean Sciences, University of California, Santa Cruz, CA 95064, USA. E-mail: tguilderson@llnl.gov
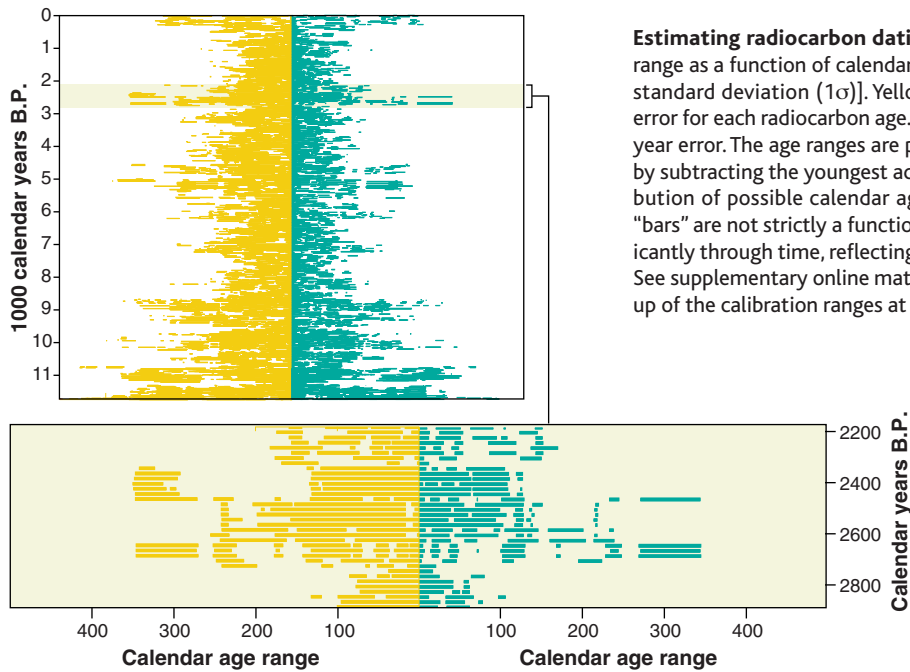
Estimating radiocarbon dating/calibration uncertainty. (Top) Calibrated age range as a function of calendar age and the uncertainty in the radiocarbon date [1 standard deviation (1σ)]. Yellow lines: Calibration 1, calculated with a ±40 year error for each radiocarbon age. Blue lines: Calibration 2, calculated assuming a ±15 year error. The age ranges are plotted against true calendar age and are calculated by subtracting the youngest acceptable age (1 standard deviation) from the distribution of possible calendar age ranges. The lengths of the calibrated age-range "bars" are not strictly a function of radiocarbon age/date precision but vary significantly through time, reflecting the strong influence of calibration curve "wiggles." See supplementary online material for the full calibration results. (**Bottom**) Close-up of the calibration ranges at 2200 to 2900 calendar years B.P.

(minimum 4 years, maximum 511 years) for calibration 2. During the most recent 500 years, the calibrated age ranges for calibration 2 are relatively low because single-year calibration data are available for that period, compared to the decadal calibration data for earlier sections.

The IntCal98 curve shows several "age plateaus" caused by variations in the atmospheric radiocarbon content. For the duration of such a plateau, the $^{14}C/^{12}C$ ratio fell at a rate equal to that of radiocarbon decay. For example, the "Golden Age of Greece" from 546 to 404 B.C. coincides with a radiocarbon plateau (~2450 radiocarbon years B.P.) that lasted nearly 350 years (see the second figure). Because of this plateau, the utility of radiocarbon dating in establishing chronologies for events between ~750 and ~400 B.C. is extremely limited. Two radiocarbon plateaus associated with the Younger Dryas (~11,900 to ~13,000 calendar years B.P.) have made it very difficult to determine whether climate change occurred synchronously across the globe during this period.

In fact, instances in which the calibrated age range is equal to or less than the analytical error in the radiocarbon age are relatively rare (<2%). Calibration of radiocarbon dates most often results in calendar age ranges that are much wider than indicated by the radiocarbon date uncertainties, resulting in an often underappreciated shortcoming of many paleoclimate time series: It is very diffi-

cult to determine absolute timing of events between independent paleoclimate records at the centennial level. Far too often, the interpretations of leads, lags, or synchronicity of paleoclimate records are not fully supported by the radiocarbon chronology.

Comparison of calibrations 1 and 2 shows that throughout much of the past 10,000 years, increased precision will reduce the calibrated age range by 20 to 50%, at least for high-quality terrestrial samples. For example, the 8200 calendar year age assigned from a Greenland ice core chronology (GISP-2) to a cold event that is widely recognized in circum-North Atlantic records (9) corresponds to 7410 radiocarbon years B.P. Calibration 1 then yields a calibrated age range of 8173 to 8325 calendar years B.P. (152 years), whereas calibration 2 gives 8167 to 8284 calendar years
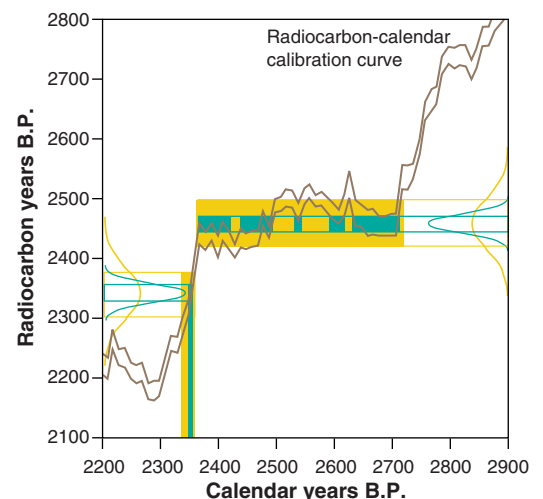
B.P. (117 years). The calibrated age ranges exceed one century because of a ~100-year plateau between 8300 and 8200 calendar years B.P.

The decreased calendar year age ranges that could be obtained from chronologies based on more precise radiocarbon dates could help to discern the temporal relationship between abrupt climate change and societal response. The collapse of the Akkadian Empire in Mesopotamia at ~3800 radiocarbon years B.P. (10) could then be calibrated to 4149 to 4231 calendar years B.P. (82 years, calibration 2), compared with 4093 to 4241 calendar years B.P. (148 years, calibration 1). Such increased precision could help to show when city-states in northern and in southern Mesopotamia were abandoned and perhaps to distinguish between climatic and societal effects.

But additional precision would not necessarily help to determine the relative roles of climate and society in the Terminal Classic Collapse of the Mayan civilization (11). The end of the collapse at ~1000 radiocarbon years B.P. (12) can be calibrated to 1003 to 1027 A.D. with calibration 2, but its beginning at 800 A.D. (~1190 radiocarbon years B.P.) yields roughly the same calibrated age range, 780 to 890 A.D., for calibrations 1 and 2.

Before 11,800 years ago, problems and difficulties still exist in deriving an accu-

A calibration example. This is an example of the influence of a radiocarbon plateau on radiocarbon calibration. The curves are 1σ Gaussian probabilities of hypothetical radiocarbon ages with ±40 (yellow, calibration 1) and ±15 (blue, calibration 2) year error bars for 2340 (left) and 2460 (right) radiocarbon years B.P. The bars and pattern-fill show the regions of the calibration curve that are intercepted by the radiocarbon ages and their 1σ uncertainties. The intercept regions are projected onto the calendar year axis for the 2340 radiocarbon age to indicate the calendar year age ranges that would be obtained from the calibration process. The variations in the calibration curve dictate that for a 2340 radiocarbon date, it would be possible to derive a decadal-scale calendar year age range. In contrast, for a 2460 radiocarbon date, the derived age range would encompass several centuries irrespective of the uncertainty in the radiocarbon date.

rate radiocarbon year–calendar year calibration curve. This problem is particularly acute prior to the last glacial maximum (about 20,000 years ago). Several data sets from various natural sources have been proposed for calibration use, but no two data sets agree sufficiently to establish a consensus (*13*).

Scientists attempting to take advantage of the available IntCal98 calibration curve to establish subcentennial resolution chronologies must become more familiar with the calibration curve and its inherent limitations. In many circumstances, radiocarbon dates on a series of carefully chosen samples will allow considerable refinement of the derived calendar ages through constraints imposed by a priori information (such as stratigraphy) or by the pattern of the radiocarbon dates relative to calibration curve variations (an approach that is sometimes

referred to as "wiggle-matching"). Even with the implementation of such methods, the establishment of reliable chronologies with centennial or better resolution will require substantial diligence and the devotion of appropriate resources to overcome the inherent limitations in the conversion of radiocarbon dates to calendar ages.

References and Notes

1. W. F. Libby, E. C. Anderson, J. R. Arnold, *Science* **109**, 227 (1949).
2. M. Stuiver, H. A. Polach, *Radiocarbon* **19**, 355 (1977).
3. M. Stuiver, P. D. Quay, *Earth Planet. Sci. Lett.* **53**, 349 (1981).
4. M. Stuiver, P. J. Reimer, *Radiocarbon* **35**, 215 (1993).
5. E. S. Deevey *et al.*, *Proc. Natl. Acad. Sci. U.S.A.* **40**, 285 (1954).
6. I. Hutchinson *et al.*, *Quat. Res.* **61**, 193 (2004).
7. M. Stuiver, H. E. Suess, *Radiocarbon* **8**, 534 (1966).
8. M. Stuiver *et al.*, *Radiocarbon* **40**, 1041 (1998).
9. P. M. Grootes, M. Stuiver, *J. Geophys. Res.* **102**, 26455 (1997).
10. H. Weiss *et al.*, *Science* **261**, 995 (1993).
11. D. A. Hodell *et al.*, *Science* **292**, 1367 (2001).
12. This simple exercise uses the tree-ring portion of the IntCal98 calibration curve. This portion is constructed entirely from Northern Hemisphere trees. However, the seasonal migration of the intertropical convergence zone will yield a mixture of Northern Hemisphere and Southern Hemisphere air in the tropics (*14*). The Northern Hemisphere–Southern Hemisphere difference averages 41±14 years between 1850 and 950 A.D. but varies from ~8 to ~80 years for any given decade (*15*).
13. P. J. Reimer, *Radiocarbon* **44**, 653 (2002).
14. J. A. Westbrook, T. P. Guilderson, P. A. Colinvaux, *IAWA Bulletin*, in press.
15. A. G. Hogg *et al.*, *Radiocarbon* **44**, 633 (2002).
16. This manuscript benefited from discussions with the IntCal 2004 and the MESH Abrupt Climate Change working groups. We thank B. Thunell for reviewing an early draft of this manuscript, and the criticisms and comments of two anonymous reviewers. Funding provided by the U.S. National Science Foundation's ESH Program (ATM-0407554) and the University of California's Lawrence Livermore National Laboratory (contract W-7405-Eng-48).

CHEMISTRY

Short and Sharp—Spectroscopy with Frequency Combs

Thomas Udem

Ever since high-resolution laser spectroscopy was introduced as a way to study atoms and molecules, many experts in the field thought that only continuous ("single-mode") lasers can resolve narrow spectral features. Much work has therefore been devoted to the construction of spectrally pure single-mode lasers. These lasers work well at infrared and visible wavelengths, but they become troublesome in the near-ultraviolet and virtually impossible to realize for even shorter wavelengths, for example in the extreme ultraviolet (10 to 100 nm).

These short wavelengths can easily be accessed with pulsed lasers through the use of nonlinear interactions. The shortest wavelength to date has been achieved with a process called high harmonic generation (HHG). (Harmonics are integer multiples of a laser frequency, that is, integer fractions of its wavelength.) However, nonlinear interactions are efficient only with short laser pulses, which cause spectral broadening of the laser. The spectral width of the laser is roughly equal to the inverse pulse duration, yielding 10^{14} Hz for a 10-femtosecond (10^{-14} s) pulse (a typical pulse duration for HHG). This is far too wide for precision experiments, where a resolution of ~10 Hz has been reached (*1, 2*).

The author is at the Max-Planck-Institut für Quantenoptik, 85748 Garching, Germany. E-mail: thu@mpq.mpg.de

On page 400 of this issue, Witte *et al.* (*3*) report an experiment that circumvents that limit. The trick is to use not just one pulse but a train of *N* coherent pulses. (This is similar to the interference of multiple light rays to form the spectrally narrow features of a grating.) The authors are not the first to record spectral lines that are narrower than the spectral width of a single pulse, but they are the first to use harmonics for that purpose.

The spectrum of a pulse train has an "envelope" that is given by the spectrum of a single pulse, but it is divided up into a series of fringes that are separated by the pulse repetition rate f_{rep} of the pulse train (see the first figure). The fringes are perfectly regular in frequency space if the pulses are perfectly regular in the time domain. The pulse train must be coherent, that is, the pulses must have a defined (nonrandom) phase relation to each other. This requirement is almost automatically fulfilled with a mode-locked laser. Such lasers emit pulse trains in which all pulses are copies of a single pulse. In the spectrum of a train of $N > 1$ pulses, the

fundamental limit of the width of a single fringe is given approximately by f_{rep}/N. For a typical mode-locked laser, this is much smaller than the spectral width of a single pulse. For $N = 3$ and $f_{rep} \sim 70$ MHz, as used by Witte *et al.* (*3*), we expect a fringe width of 70/3 MHz = 23 MHz. Indeed, that is roughly the linewidth observed by the authors [see figure 3 of (*3*)]. It is still large compared to the requirements of high-resolution spectroscopy, but improvements by many orders of magnitude should be possible.

For these improvements to become a reality, one must shine more pulses on the atoms or molecules. In this case, the fringes turn into sharp spikes that can be as narrow as in a well-stabilized single-mode laser (*4*). Such a series of delta-shaped spikes is usually called a frequency comb and can be used to measure the frequency of any of the spikes relative to an atomic clock (a very
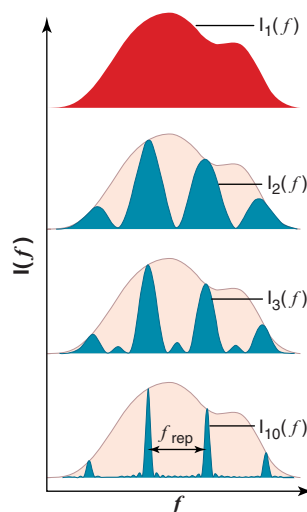
How to narrow the linewidth. The spectrum of a train of *N* pulses, $I_N(f)$, is shown schematically for some values of *N*. The single-pulse spectrum (red curve; repeated as a pink "envelope" in the subsequent spectra) is as broad as the inverse pulse duration. Multiple pulsing causes fringes (blue curves) with a linewidth of f_{rep}/N to appear. For a large number of pulses, the spectrum resembles a series of delta-shaped spikes, which are the modes of the frequency comb, that is, the modes of the laser. For a laser with $f_{rep} = 100$ MHz and a pulse duration of 10 fs, one expects 1 million modes (or fringes) to appear.